JOC The Journal of Organic Chemistry

Article

pubs.acs.org/joc

Merging Two Strategies for Mixed-Sequence Recognition of Double-Stranded DNA: Pseudocomplementary Invader Probes

Brooke A. Anderson and Patrick J. Hrdlicka*

Department of Chemistry, University of Idaho, Moscow, Idaho 83844-2343, United States

Supporting Information

ABSTRACT: The development of molecular strategies that enable recognition of specific double-stranded DNA (dsDNA) regions has been a longstanding goal as evidenced by the emergence of triplex-forming oligonucleotides, peptide nucleic acids (PNAs), minor groove binding polyamides, and—more recently—engineered proteins such as CRISPR/Cas9. Despite this progress, an unmet need remains for simple hybridization-based probes that recognize specific mixed-sequence dsDNA regions under physiological conditions. Herein, we introduce *pseudocomplementary Invader* probes as a step in this direction. These double-stranded probes are chimeras between pseudocomplementary DNA (pcDNA) and Invader probes, which are activated for mixed-sequence dsDNA-recognition through the introduction of pseudocomplementary base pairs comprised of 2-thiothymine and 2,6-diaminopurine, and +1 interstrand zipper arrangements of intercalator-functionalized nucleotides, respectively. We demonstrate that certain pseudocomplementary Invader probe designs result in very efficient and specific recognition of model dsDNA targets in buffers of high ionic strength. These chimeric probes, therefore, present themselves as a promising strategy for mixed-sequence recognition of dsDNA targets for applications in molecular biology and nucleic acid diagnostics.

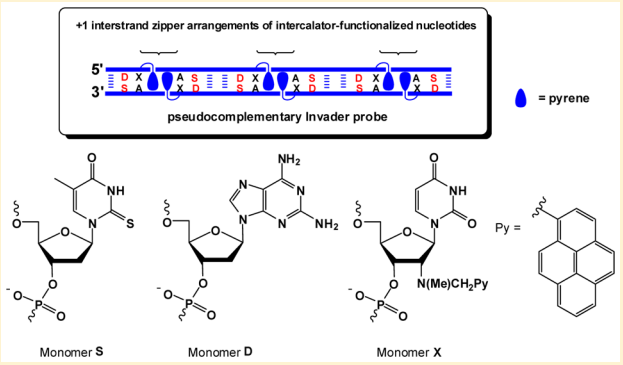

INTRODUCTION

Probes capable of recognizing specific mixed-sequence double-stranded DNA (dsDNA) regions have been long-sought-after as they can be developed into tools that enable modulation of gene expression at the transcriptional level, gene editing, and detection of specific genetic signatures. Early examples of dsDNA-targeting probes include triplex-forming oligonucleotides[1] (TFOs) and peptide nucleic acids[2,3] (PNAs), as well as minor groove binding polyamides.[4,5] Unfortunately, only a subset of the possible target regions is available for recognition by these probes due to requirements for exclusive purine content (TFOs/PNAs) or short target regions (polyamides). Consequentially, significant efforts have been devoted to develop alternative approaches, which has resulted in TFOs and PNAs with reduced target site limitations.[6−11] More recently, engineered proteins[12,13] such as zinc finger nucleases, transcription activator-like effector nucleases (TALENs) and—in particular—CRISPR/Cas9 systems,[14] have gained a tremendous amount of attention, despite mounting concerns regarding recognition specificity and cellular delivery.[15] Another class of compounds that has emerged from these efforts are the so-called pseudocomplementary DNA and PNA (pcDNA/pcPNA),[16−18] in which a short DNA or PNA duplex is modified to contain pseudocomplementary base pairs between 2-thiothymine and 2,6-diaminopurine (Figure 1a). The steric clash between the 2-thio and the 2-amino group perturbs and weakens the hydrogen bonding between these moieties, resulting in a destabilized probe duplex. In contrast, 2-thiothymine and 2,6-diaminopurine form stable base pairs with canonical adenine and thymine, respectively. The difference in thermodynamic stability between probe duplexes and duplexes between individual probe strands and complementary DNA (cDNA) allows for double-duplex invasion of dsDNA target regions under certain conditions (Figure 1b). Thus, pcDNA can recognize terminal target regions, while pcPNA also recognize internal target regions of DNA duplexes, albeit at low ionic strengths. However, a recent study has suggested that recognition of mixed-sequence dsDNA regions by pcPNA may be possible under the highly viscous conditions found in the nucleus.[19]

We,[20] and later others,[21] have pursued an alternative strategy for the construction of energetically activated double-stranded probes for recognition of mixed-sequence dsDNA regions, which is based on forced intercalation of aromatic moieties. Our *Invader* probes are short DNA duplexes containing +1 interstrand zipper arrangements of intercalator-functionalized nucleotides (Figure 1c; for a definition of the zipper nomenclature, see Experimental Section). This motif, which we denote as an *energetic hotspot*, forces two intercalators into

Received: February 19, 2016
Published: March 21, 2016

DOI: 10.1021/acs.joc.6b00369
J. Org. Chem. 2016, 81, 3335−3346

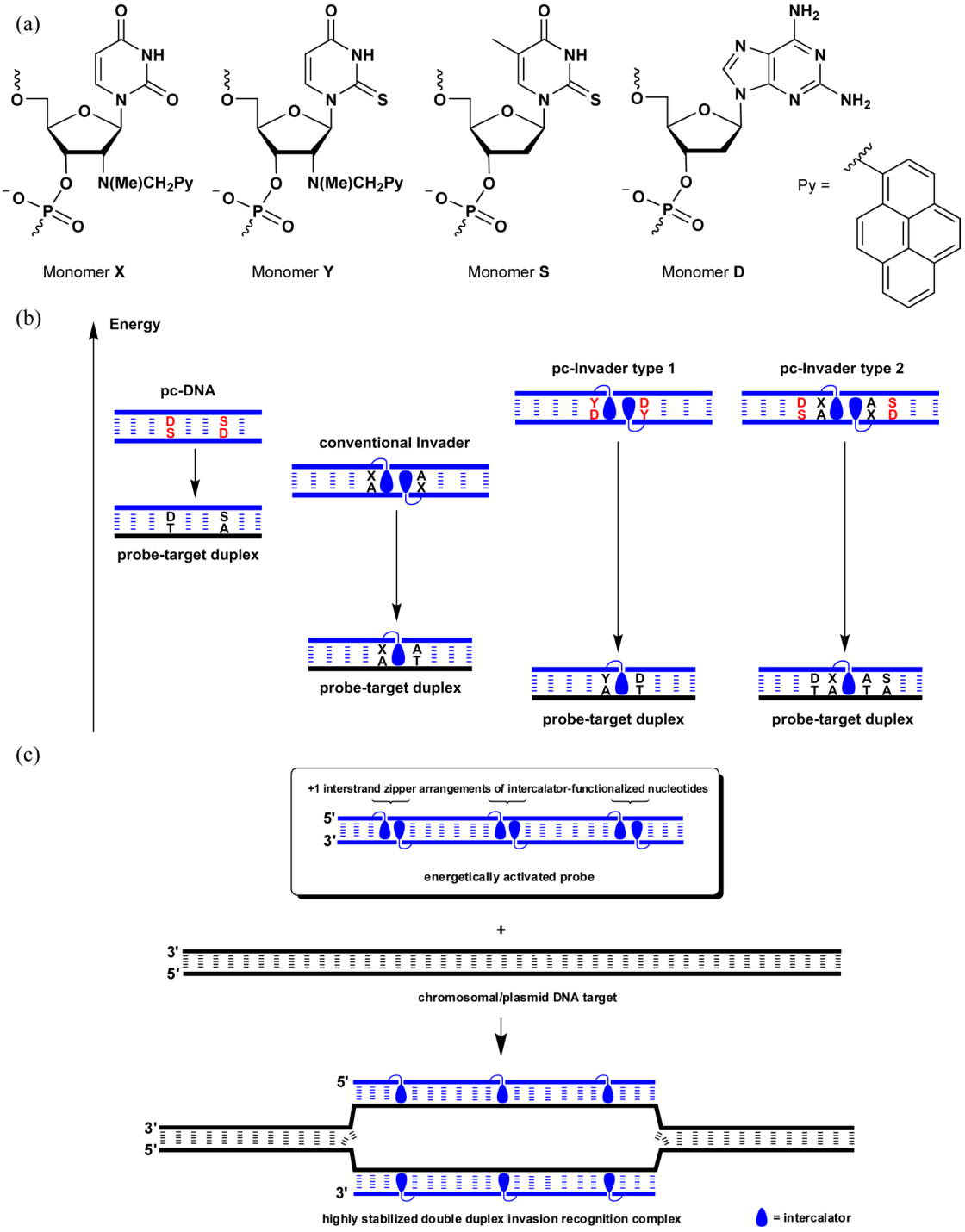

Figure 1. (a) Structures of monomers used herein. (b) Representation of energy levels of different dsDNA-targeting probes and the corresponding duplexes with cDNA (only one probe-target duplex is shown). Pseudocomplementary base-pairs are shown in red. Droplets denote intercalators. Note, the large difference in energy between pc-Invader:cDNA duplexes and pc-Invader probe duplexes. (c) Illustration of Invader-mediated recognition of dsDNA target regions.

the same region of the duplex, resulting in unwinding and destabilization[22,23] as the nearest neighbor exclusion principle[24] is violated. According to this principle, the space between the two nearest base pairs on either side of a bound intercalator, will not be bound by a second intercalator due to limitations in local helix expandability (every intercalation event unwinds the duplex by ~3.4 Å),[25] and/or to avoid disruption of highly stable stacking interactions between the first bound intercalator and neighboring nucleobases.[26] On the other hand, each of the two strands comprising an Invader probe display very high affinity toward cDNA since the intercalators stack strongly with the neighboring base pairs, acting as molecular glue (Figure 1c).[22,27] We have previously demonstrated that the differences in thermostability between Invader probes and probe-cDNA duplexes can drive mixed-sequence recognition of isosequential DNA duplexes,[20,22,27,28] DNA hairpins,[22] and chromosomal DNA targets.[29]

DOI: 10.1021/acs.joc.6b00369
J. Org. Chem. 2016, 81, 3335−3346

Scheme 1. Synthesis of Target Phosphoramidite 6[a]

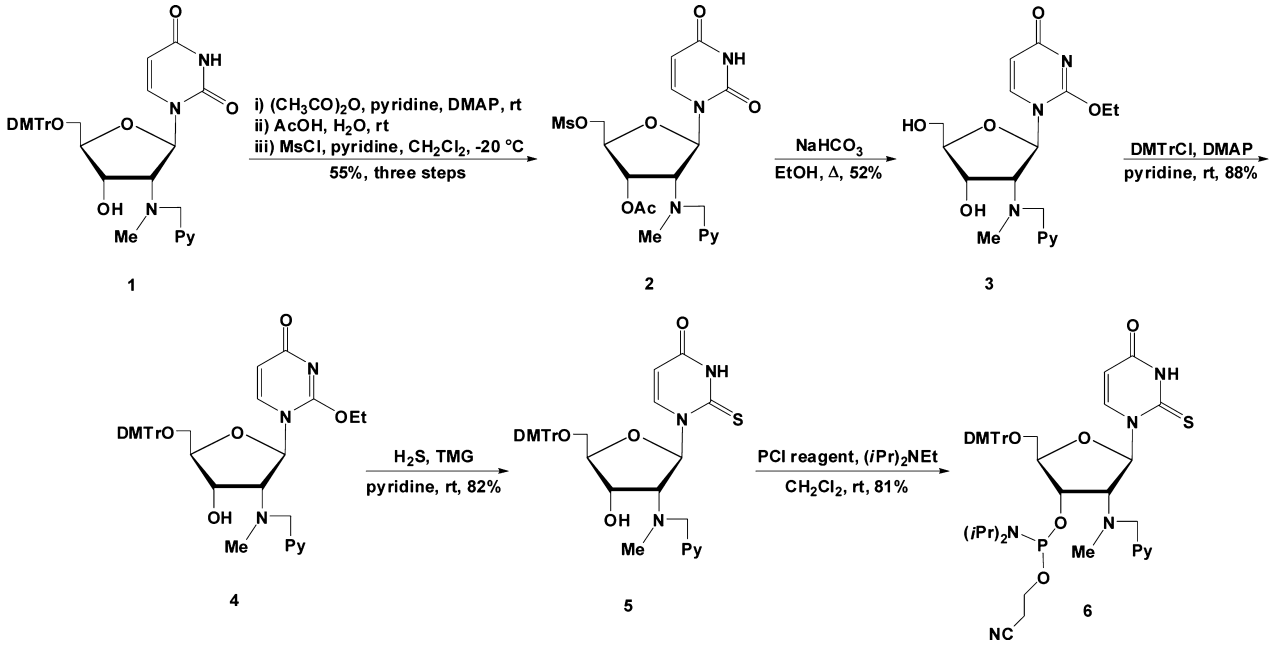

[a]DMTr = 4,4′-dimethoxytrityl; Py = pyren-1-yl; Ms = methanesulfonyl; TMG = 1,1,3,3-tetramethylguanidine; PCl reagent = 2-cyanoethyl-*N*,*N*-diisopropylchlorophosphoramidite.

Initially, 2′-*N*-(pyren-1-yl)-2′-amino-α-L-LNA (Locked Nucleic Acid) monomers were used to construct the energetic hotspots of Invader probes.[20,22,27] However, the challenging synthesis of these building blocks, prompted us to conduct a search for more feasible structural and functional mimics, which, among others, resulted in the identification of 2′-*N*-(pyren-1-yl)methyl-2′-*N*-methyl-2′-aminouridine monomer **X** as a next-generation Invader modification (Figure 1a).[22] Access to building blocks that are based on simpler sugar scaffolds has facilitated extensive structure−property relationship studies aiming at improving the recognition efficiency of Invader probes.[30−36]

In the present study, we set out to study if the dsDNA-recognition potential of Invader probes can be increased further through incorporation of pseudocomplementary base pairs. We hypothesized that these chimeric *pseudocomplementary Invader probes* will be more energetically labile, yet form even more stable duplexes with cDNA than either canonical Invader or pcDNA probes, leading to more favorable energetics for dsDNA-recognition (Figure 1b). Toward this end, two different approaches were followed. In the first, we wanted to integrate the intercalator as part of a pseudocomplementary nucleotide, which led to the identification of 2′-*N*-(pyren-1-yl)methyl-2′-*N*-methyl-2′-amino-2-thiouridine monomer **Y** as a target (Figure 1a). Incorporation of this monomer in a +1 interstrand zipper arrangement opposite of conventional 2,6-diaminopurine DNA **D** monomers would furnish a double-stranded probe with a pseudocomplementary energetic hotspot (**DY** probes) (Figure 1b). In the second approach, we separated the two key structural features by using conventional 2-thiothymine DNA monomer **S** and 2,6-diaminopurine DNA monomer **D**, alongside energetic hotspots comprised of the conventional Invader monomer **X** (**DSX** probes) (Figure 1b). We demonstrate that the latter type of probes is particularly interesting for dsDNA-recognition applications.

RESULTS AND DISCUSSION

Synthesis of N2′-Pyrene-Functionalized 2-Thiouridine Phosphoramidite. The key 2′-*N*-(pyren-1-yl)methyl-2′-*N*-methyl-2′-amino-2-thiouridine phosphoramidite **6** was obtained from known nucleoside **1**, following a similar general strategy as was used for the synthesis of 2′-*O*-[2-(methoxy)ethyl]-2-thiothymidine (Scheme 1).[37] Thus, nucleoside **1**—obtained in 61% yield over six steps from uridine[32]—was first subjected to a sequence of protecting group manipulations, i.e., 3′-*O*-acetylation, 5′-*O*-detritylation and 5′-*O*-methanesulfonylation, to afford nucleoside **2** in 55% yield over three steps. Prolonged refluxing in anhydrous ethanol in the presence of sodium bicarbonate,[37] results in the formation of 2-*O*-ethyluridine derivative **3** in 52% yield, presumably via a nucleophilic opening of an O2,O5′-anhydrouridine intermediate. Subsequent O5′-dimethoxytritylation of **3** using standard conditions affords nucleoside **4** in 88% yield, which upon treatment with H_2S-saturated pyridine in the presence of 1,1,3,3-tetramethylguanidine[38] provides 2-thiouridine derivative **5** in 82% yield. Treatment of nucleoside **5** with 2-cyanoethyl-*N*,*N*-diisopropyl-chlorophosphoramidite and *N*,*N*-diisopropylethylamine affords target phosphoramidite **6** in 81% yield, corresponding to an overall yield of ∼17% from nucleoside **1**.

Synthesis of Modified ONs. Phosphoramidite **6** was used to incorporate monomer **Y** into oligodeoxyribonucleotides (ONs) via automated solid-phase DNA synthesis. Extended hand-coupling (15 min) and the use of 4,5-dicyanoimidazole as an activator resulted in stepwise coupling yields of ∼95%. ONs modified with monomer **X** were synthesized as previously described (15 min coupling, 5-[3,5-bis(trifluoromethyl)-phenyl]-1*H*-tetrazole as an activator, ∼99% coupling yield).[39] The corresponding phosphoramidites of monomers **S** and **D** were obtained from commercial sources and incorporated into ONs using the conditions for incorporation of monomer **Y** (stepwise coupling yields >95%). To prevent desulfurization in ONs modified with **Y** or **S** monomers, nucleotide phosphite to

DOI: 10.1021/acs.joc.6b00369
J. Org. Chem. 2016, 81, 3335−3346

phosphate oxidation was performed using *tert*-butylhydroperoxide/CH_3CN/H_2O (10 min) rather than the standard aqueous iodine solution.[40] The identity and purity of the modified ONs were established through MALDI-TOF (Table S1) and ion-pair reverse-phase HPLC (>90% purity unless otherwise noted), respectively.

Thermal Denaturation Properties of Y- or DY-Modified Duplexes. Pyrene-functionalized 2-thiouracil monomer **Y** was incorporated into the same 9-mer mixed-sequence ONs that was previously used for evaluation of Invader monomer **X**.[32] Thermal denaturation temperatures (T_m's) of duplexes between **Y**-modified ONs and cDNA or cRNA were determined in a medium salt phosphate buffer ([Na^+] = 110 mM) and compared relative to unmodified and corresponding **X**-modified duplexes. The resulting denaturation curves display the expected monophasic sigmoidal transitions (Figure S1). Duplexes between **Y1**−**Y4** and cDNA are significantly more stable than unmodified reference duplexes (ΔT_m between +2.5 and +11.5 °C, Table 1), whereas heteroduplexes with cRNA are much less stable (ΔT_m between −6.5 to +2.5 °C, Table S2). ONs in which **Y** monomers are flanked by 3′-purines result in greater duplex stabilization than ONs with 3′-flanking pyrimidines (e.g., compare ΔT_m's for **Y1** and **Y3**, Table 1). This sequence dependence, along with the prominent DNA selectivity (Table S3), is typical for ONs modified with intercalating pyrene moieties.[22,41] Surprisingly, **Y**-modified ONs form slightly less stable duplexes with cDNA than their **X**-modified counterparts (compare T_m's of **X1**−**X4** and **Y1**−**Y4**, Table 1), which suggests that the binding modes responsible for the stabilizing contributions of the pyrene and 2-thiouracil moieties are not fully compatible.

Table 1. Thermal Denaturation Temperatures of Duplexes between X-, Y-, DY-, or D-Modified ONs and cDNA[a]

ON	sequence	ΔT_m (°C)
X1[b]	5′-GTG A**X**A TGC	+15.0
X2[b]	3′-CAC **X**AT ACG	+1.5
X3[b]	3′-CAC TA**X** ACG	+15.0
X4[b]	3′-CAC **X**A**X** ACG	+14.0
Y1	5′-GTG A**Y**A TGC	+11.5
Y2	3′-CAC **Y**AT ACG	+2.5
Y3	3′-CAC TA**Y** ACG	+11.0
Y4	3′-CAC **Y**A**Y** ACG	+10.0
DY1	5′-GTG A**YD** TGC	+16.0
DY2	5′-GTG **DY**A TGC	+13.0
DY3	3′-CAC **YD**T ACG	+3.5
DY4	3′-CAC T**DY** ACG	+16.0
D1	5′-GTG **D**TA TGC	+1.0
D2	5′-GTG AT**D** TGC	+2.0
D3	3′-CAC T**D**T ACG	+3.0
D4	5′-GTG **D**T**D** TGC	+5.0

[a]ΔT_m = change in T_m relative to reference duplex **DNA1**:**DNA2** (T_m ≡ 29.5 °C), where **DNA1**: 5′-GTG ATA TGC and **DNA2**: 3′-CAC TAT ACG. T_m's are determined as the maximum of the first derivative of melting curves (A_{260} vs T) recorded in medium salt phosphate buffer ([Na^+] = 110 mM, [Cl^-] = 100 mM, pH 7.0 (NaH_2PO_4/Na_2HPO_4)), using 1.0 μM of each strand. Reported T_m's are averages of at least two measurements within 1.0 °C; A = adenin-9-yl DNA monomer, C = cytosin-1-yl DNA monomer, G = guanin-9-yl DNA monomer, and T = thymin-1-yl DNA monomer. For structures of monomers **X**, **Y**, and **D**, see Figure 1a. [b]Data previously reported in ref 32.

To generate Invader probes with pseudocomplementary energetic hotspots, we synthesized ONs in which 2-amino-2′-deoxyadenosine monomers flank monomer **Y** (i.e., the **DY** series). Replacing regular 2′-deoxyadenosines with **D** monomers increases the cDNA/cRNA affinity of **Y**-modified ONs by 1−5 °C, presumably due to stabilization from the extra hydrogen bond in **D**:T base pairs relative to normal A:T pairs (e.g., compare ΔT_m for **Y1** and **DY1**, Table 1 and Table S2). Similar relative increases in cDNA affinity are observed when 2′-deoxyadenosines are replaced with **D** monomers in otherwise unmodified ONs (see ΔT_m for **D1**−**D4** vs cDNA, Table 1), which is in agreement with previous studies.[42,43]

Next, we set out to study DNA duplexes with different interstrand zipper arrangements of **Y** monomers and **DY** segments to identify probe architectures that are strongly activated for dsDNA-recognition. As expected from our previous studies on Invader probes,[32] **Y1**:**Y3**, which features a +1 interstrand zipper of **Y** monomers, is much more thermolabile than **Y1**:**Y2** featuring a −1 interstrand zipper (Table 2), or duplexes between **Y**-modified ONs and cDNA (Table 1). The destabilization is likely a consequence of the nearest neighbor exclusion principle[25,26] being violated. In line with our hypothesis, introduction of a 2,6-diaminopurine **D** monomer opposite of the pyrene-functionalized 2-thiouracil **Y** monomer, decreases the T_m's of the duplexes (e.g., compare ΔT_m of **DY2**:**DY3** and **Y1**:**Y2**, Table 2). Interestingly, the destabilizing effect of the pseudocomplementary base pairs is more pronounced when the **Y** monomers are positioned in a −1 zipper orientation (drop in T_m of 9.5 °C from **Y1**:**Y2** to **DY2**:**DY3**, relative to drop of 2.0 °C from **Y1**:**Y3** to **DY1**:**DY4**, Table 2). This indicates that the pseudocomplementary energetic hotspot architecture of **DY1**:**DY4** does not fully harness the activating effects from both structural elements.

The T_m-based conclusions were largely corroborated by the Gibbs free energies associated with duplex formation, which were derived from denaturation curves via line fitting (Table 2).[44] Thus: (i) Duplexes between **Y**-modified ONs and cDNA are much more stable than unmodified reference duplexes ($\Delta\Delta G^{293}$ between −16 and −7 kJ/mol, first and second ΔG^{293} columns, Table 2) due to more favorable enthalpy ($\Delta\Delta H$ between −76 and −44 kJ/mol, Table S7). (ii) In comparison, the corresponding **X**-modified duplexes are slightly more stable, while the **D**-modified duplexes are far less stable (e.g., compare $\Delta\Delta G^{293}$ for **Y1**:cDNA, **X1**:cDNA and **D1**:cDNA, Table 2). (iii) Duplexes between ONs with **DY** motifs and cDNA are generally less stable than the corresponding **Y**-modified duplexes (e.g., compare $\Delta\Delta G^{293}$ for **Y1**:cDNA and **DY2**:cDNA, Table 2). This contrasts the T_m-based conclusions (Table 1), but likely reflects the different entropies of these duplexes (Table S8), leading to different temperature dependencies of the Gibbs free energies. (iv) Formation of **Y1**:**Y3** (+1 zipper) is less thermodynamically favorable than **Y1**:**Y2** (−1 zipper) (third ΔG^{293} column, Table 2). (v) Duplexes with pseudocomplementary energetic hotspots are slightly less stable than the corresponding duplexes featuring only regular energetic hotspots (e.g., compare ΔG^{293} for **DY1**:**DY4** and **Y1**:**Y3**, Table 2). The energetic nature of **DY1**:**DY4** is the result of particularly unfavorable enthalpy ($\Delta\Delta H$ = +95 kJ/mol, Table S7), likely reflecting a violation of the nearest neighbor exclusion principle and concomitant formation of destabilizing

DOI: 10.1021/acs.joc.6b00369
J. Org. Chem. 2016, 81, 3335−3346

Table 2. Biophysical Properties of X-, Y- or DY-Modified DNA Duplexes[a]

ON	ZP	sequence	T_m (°C)	$\Delta G^{293}[\Delta\Delta G^{293}]$ (kJ/mol) upper ON vs cDNA	lower ON vs cDNA	probe duplex	ΔG^{293}_{rec} (kJ/mol)	λ_{max} (nm)
X1 **X2**	-1	5′-GTG A**X**A TGC 3′-CAC **X**AT ACG	42.5	−65 ± 1 [−20]	−48 ± 1 [−3]	−54 ± 1 [−9]	−14	352
X1 **X3**	+1	5′-GTG A**X**A TGC 3′-CAC TA**X** ACG	28.5	−65 ± 1 [−20]	−64 ± 1 [−19]	−44 ± 0 [+1]	−40	345
Y1 **Y2**	−1	5′-GTG A**Y**A TGC 3′-CAC **Y**AT ACG	39.5	−61 ± 1 [−16]	−52 ± 1 [−7]	−54 ± 0 [−9]	−14	353
Y1 **Y3**	+1	5′-GTG A**Y**A TGC 3′-CAC TA**Y** ACG	28.5	−61 ± 1 [−16]	−59 ± 1 [−14]	−46 ± 0 [−1]	−29	347
DY2 **DY3**	−1	5′-GTG **DY**A TGC 3′-CAC **YD**T ACG	30.0	−56 ± 1 [−11]	−48 ± 1 [−3]	−46 ± 1 [−1]	−13	352
DY1 **DY4**	+1	5′-GTG A**YD** TGC 3′-CAC T**DY** ACG	26.5	−60 ± 1 [−15]	−61 ± 2 [−16]	−42 ± 1 [+3]	−34	350
D1 **Y2**	–	5′-GTG **D**TA TGC 3′-CAC **Y**AT ACG	24.0	−47 ± 1 [−2]	−52 ± 1 [−7]	−43 ± 1 [+2]	−11	352
Y1 **D3**	–	5′-GTG A**Y**A TGC 3′-CAC T**D**T ACG	32.5	−61 ± 1 [−16]	−49 ± 0 [−4]	−51 ± 1 [−6]	−14	352
D2 **Y3**	–	5′-GTG AT**D** TGC 3′-CAC TA**Y** ACG	33.5	−48 ± 0 [−3]	−59 ± 1 [−14]	−51 ± 0 [−6]	−11	353
D4 **Y4**	–	5′-GTG **D**T**D** TGC 3′-CAC **Y**A**Y** ACG	24.5	−51 ± 1 [−6]	−58 ± 0 [−13]	−44 ± 0 [+1]	−20	353

[a]ZP = zipper. For conditions of thermal denaturation, see Table 1. $\Delta\Delta G^{293}$ is measured relative to ΔG^{293} for **DNA1**:**DNA2** = −45 kJ/mol. ΔG^{293}_{rec} (**ON$_A$**:**ON$_B$**) = ΔG^{293} (**ON$_A$**:cDNA) + ΔG^{293} (cDNA:**ON$_B$**) − ΔG^{293} (**ON$_A$**:**ON$_B$**) − ΔG^{293} (dsDNA). "±" denotes standard deviation. Absorption spectra were recorded at T = 10 °C using each strand at 1.0 μM concentration in T_m buffer. Data for **X1**:**X2** and **X1**:**X3** are from ref 32 and are included to facilitate comparison.

pseudocomplementary base pairs. (vi) pc-DNA without any energetic hotspots range between being slightly more stable to slightly less stable than unmodified duplexes (e.g., see $\Delta\Delta G^{293}$ for **D1**:**Y2** and **Y1**:**D3**, Table 2).

Consequentially, +1 zipper duplex **Y1**:**Y3** is much more energetically activated than −1 zipper duplex **Y1**:**Y2**, as gauged by the free energy available for recognition of isosequential dsDNA targets ΔG^{293}_{rec} (ON$_A$:ON$_B$) = ΔG^{293} (ON$_A$:cDNA) + ΔG^{293} (cDNA:ON$_B$) − ΔG^{293} (ON$_A$:ON$_B$) − ΔG^{293} (dsDNA), where ON$_A$:ON$_B$ denotes a double-stranded probe and "dsDNA" is the isosequential dsDNA target for ON$_A$:ON$_B$ (compare ΔG^{293}_{rec} for **Y1**:**Y2** and **Y1**:**Y3**, Table 2). **DY1**:**DY4**, featuring a pseudocomplementary energetic hotspot, is slightly more energetically activated for dsDNA-recognition than **Y1**:**Y3** (compare ΔG^{293}_{rec} for **DY1**:**DY4** and **Y1**:**Y3**, Table 2). As expected, **DY2**:**DY3**, which also features two pseudocomplementary base pairs but has an −1 interstrand zipper arrangement of **Y** monomers, is far less activated for dsDNA-recognition (compare ΔG^{293}_{rec} for **DY2**:**DY3** and **DY1**:**DY4**, Table 2). pc-DNA without energetic hotspots are also far less activated for dsDNA-recognition (e.g., compare ΔG^{293}_{rec} of **Y1**:**D3** and **DY1**:**DY4**, Table 2).

Unexpectedly, **DY1**:**DY4** has lower thermodynamic dsDNA-recognition potential than conventional Invader probe **X1**:**X3** (compare ΔG^{293}_{rec} for **DY1**:**DY4** and **X1**:**X3**, Table 2), which likely is due to two factors: (i) intercalation of the pyrene moieties perturbs the local duplex geometry, which weakens the normally stabilizing base pairs between 2,6-diaminopurine:thymine (**D**:T) and 2-thiouracil:adenine (**Y**:A), leading to lower-than-expected cDNA-affinity of **DY**-modified ONs (e.g., compare ΔG^{293} for **X1**:cDNA, **Y1**:cDNA and **DY1**:cDNA, Table 2), and (ii) +1 interstrand zipper arrangements of nucleotide monomers with intercalating pyrene moieties perturb local duplex geometries,[31] which, in turn, are likely to reduce the steric clash between 2,6-diaminopurine and 2-thiouracil normally occurring in pseudocomplementary base pairs, resulting in less pronounced probe destabilization. It is also possible that the pseudocomplementary base pairs of **DY1**:**DY4** interfere with the forced and destabilizing intercalation of the two pyrene moieties; this is supported by the UV−vis absorption characteristics of **DY1**:**DY4**. Normally, DNA duplexes with +1 interstrand zipper motifs of intercalating pyrene-functionalized monomers exhibit markedly blue-shifted pyrene absorption relative to DNA duplexes with other interstrand zipper motifs,[31,32,34] which is indicative of reduced pyrene-nucleobase interactions[45] due to a locally perturbed duplex geometry (e.g., compare λ_{max} for **X1**:**X3** relative to **X1**:**X2**, Table 2). The same trend is observed for **Y1**:**Y3** (compare λ_{max} for **Y1**:**Y3** relative to **Y1**:**Y2**), but the trend is less pronounced for **DY1**:**DY4** (compare λ_{max} for

DOI: 10.1021/acs.joc.6b00369
J. Org. Chem. 2016, 81, 3335−3346

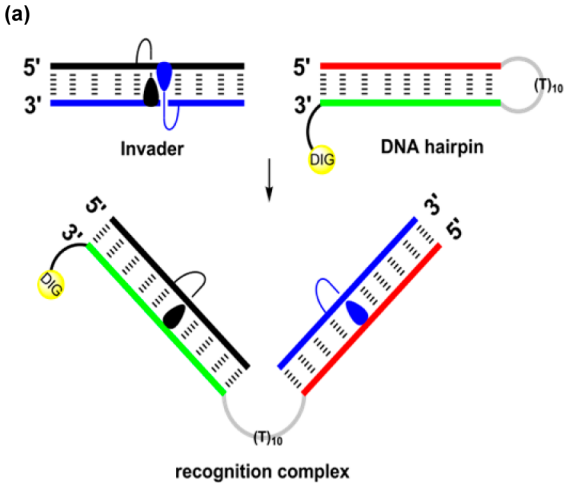

(b)

HP	Sequence	T_m (°C)
DH1	5' - GTGATATGC (T)10 3' - CACTATACG	57.0
DH2	5' - GTGAAATGC (T)10 3' - CACTTTACG	58.5
DH3	5' - GTGAGATGC (T)10 3' - CACTCTACG	62.5
DH4	5' - GTGACATGC (T)10 3' - CACTGTACG	63.5
DH5	5' - GTGATTTGC (T)10 3' - CACTAAACG	59.0
DH6	5' - GTGATGTGC (T)10 3' - CACTACACG	63.5
DH7	5' - GTGATCTGC (T)10 3' - CACTAGACG	62.5

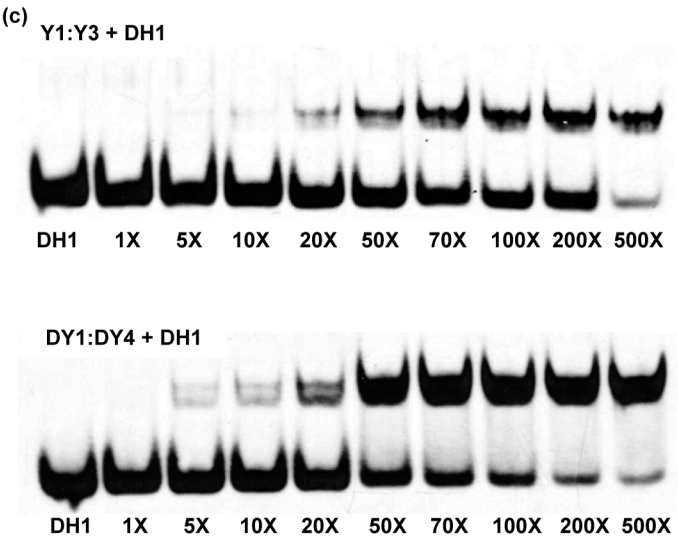

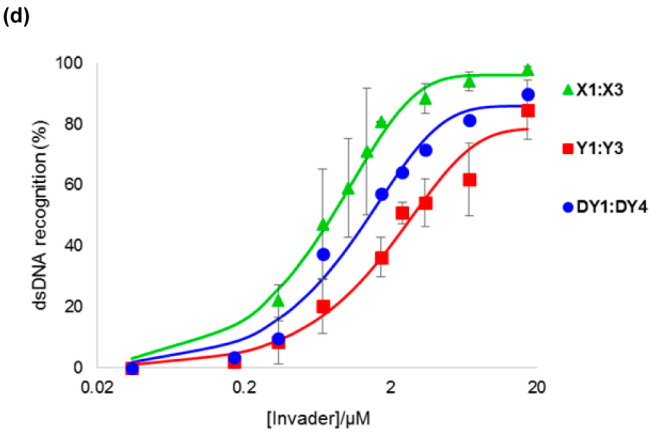

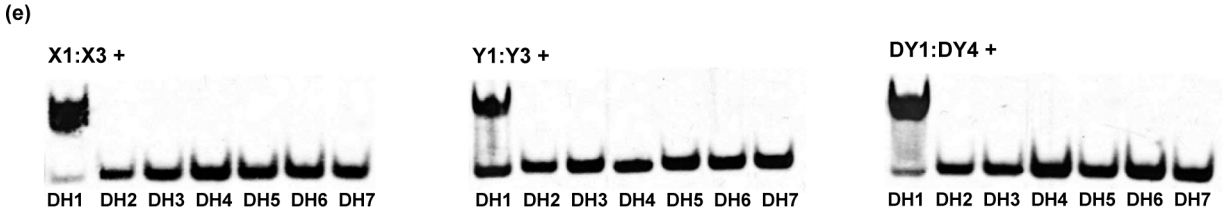

Figure 2. Recognition of DNA hairpins using Invader probes. (a) Illustration of recognition process; (b) sequences and thermal denaturation temperatures of DNA hairpins with isosequential (**DH1**) or nonisosequential stems (**DH2**–**DH7**); underlined nucleotides indicate sequence deviations relative to probes; (c) representative electrophoretograms of recognition of **DH1** using 1- to 500-fold molar excess of **Y1**:**Y3** or **DY1**:**DY4**; (d) dose–response curves (average of at least three independent experiments; error bars represent standard deviation); (e) electrophoretograms illustrating incubation of **DH1**–**DH7** with 200-fold molar excess of **X1**:**X3**, **Y1**:**Y3**, or **DY1**:**DY4**. Experimental conditions for electrophoretic mobility shift assay: separately preannealed targets (34.4 nM) and probes (variable concentrations) were incubated for 12–16 h at ambient temperature in 1X HEPES buffer (50 mM HEPES, 100 mM NaCl, 5 mM $MgCl_2$, 10% sucrose, 1.4 mM spermine tetrahydrochloride, pH 7.2) and then resolved on 16% nondenaturing PAGE (70 V, 2.5 h, ~4 °C) using 0.5× TBE as a running buffer (45 mM Tris, 45 mM boric acid, 1 mM EDTA); DIG: digoxigenin.

DY1:**DY4** relative to **DY2**:**DY3**), indicating that **DY1**:**DY4** is not strongly perturbed.

Recognition of DNA Hairpins Using DY Probes. On the basis of the observed ΔG^{293}_{rec} values, we decided to determine the dsDNA-recognition properties of **Y1**:**Y3** and **DY1**:**DY4** relative to benchmark Invader **X1**:**X3** using an electrophoretic mobility shift assay from our earlier studies.[22] Thus, a digoxigenin (DIG) labeled DNA hairpin (DH)—comprised of a 9-mer double-stranded mixed-sequence stem, which is linked by a T_{10} loop—was used as a model dsDNA target (Figure 2a and 2b). Room temperature incubation of **DH1** with **Y1**:**Y3**, **DY1**:**DY4**, or **X1**:**X3** in a HEPES buffer of considerable ionic strength, results in dose-dependent formation of a ternary recognition complex as evidenced by the emergence of a slower migrating band on nondenaturing PAGE gels (Figure 2c). Nonlinear regression fits of dose–response curves reveal that **X1**:**X3**, **Y1**:**Y3**, and **DY1**:**DY4** have C_{50} values of ~0.8 μM, ~2.8 μM, and ~1.5 μM, respectively (Figure 2d), which mirrors the trend in ΔG^{293}_{rec} values (Table 2).

The binding specificities of **Y1**:**Y3**, **DY1**:**DY4**, and **X1**:**X3** were examined by incubating a 200-fold molar excess of the probes with DNA hairpins **DH2**–**DH7**, which deviate in the

DOI: 10.1021/acs.joc.6b00369
J. Org. Chem. 2016, 81, 3335–3346

Table 3. Thermal Denaturation and Thermodynamic Properties of X-, DY-, DSX-, and DS-Modified Duplexes[a]

ON	sequence	ΔT_m (°C) upper ON vs cDNA	ΔT_m (°C) lower ON vs cDNA	ΔT_m (°C) probe duplex	$\Delta G^{293}[\Delta\Delta G^{293}]$ (kJ/mol) upper ON vs cDNA	$\Delta G^{293}[\Delta\Delta G^{293}]$ (kJ/mol) lower ON vs cDNA	$\Delta G^{293}[\Delta\Delta G^{293}]$ (kJ/mol) probe duplex	ΔG^{293}_{rec} (kJ/mol)
DSX1 **DSX2**	5′-GGTA T**D**X**S**A GGC 3′-CCAT A**S**A**X**D**T** CCG	+14.0	+14.0	−2.0	−76 ± 1 [−15]	−78 ± 1 [−17]	−52 ± 0 [+9]	−41
DSX3 **DSX4**	5′-GGTA **S**A**X**ATD GGC 3′-CCAT **D**TA**X**A**S** CCG	+15.0	+14.0	−3.0	−80 ± 1 [−19]	−77 ± 2 [−16]	−52 ± 0 [+9]	−44
DY5 **DY6**	5′-GGTA TA**YD**TA GGC 3′-CCAT ATD**Y**AT CCG	+10.0	+10.0	−1.5	−74 ± 2 [−13]	−73 ± 1 [−12]	−55 ± 1 [+6]	−31
X5 **X6**	5′-GGTA TA**X**ATA GGC 3′-CCAT ATA**X**AT CCG	+11.0	+12.0	−0.5	−76 ± 2 [−15]	−78 ± 1 [−17]	−59 ± 0 [+2]	−34
SD1 **SD2**	5′-GGTA TA**SD**TA GGC 3′-CCAT ATD**S**AT CCG	+3.5	+2.5	−8.0	−64 ± 1 [−3]	−64 ± 1 [−3]	−50 ± 1 [+11]	−17
SD3 **SD4**	5′-GGTA T**D**TA**S**A GGC 3′-CCAT A**S**ATD**T** CCG	+3.0	+2.5	−9.0	−65 ± 2 [−4]	−64 ± 1 [−3]	−50 ± 1 [+11]	−18
SD5 **SD6**	5′-GGTA **S**ATATD GGC 3′-CCAT **D**TATA**S** CCG	+4.0	+3.0	−8.0	−67 ± 1 [−6]	−65 ± 0 [−4]	−51 ± 0 [+10]	−20

[a] ΔT_m = change in T_m relative to reference duplexes **DNA3**:**DNA4** ($T_m \equiv 37.5$ °C), where **DNA3**: 5′-GGTA TATATA GGC, **DNA4**: 3′-CCAT ATATAT CCG. $\Delta\Delta G^{293}$ is measured relative to ΔG^{293} for **DNA3**:**DNA4** = −61 kJ/mol. For definition of ΔG^{293}_{rec} see Table 2. "±" denotes standard deviation. For experimental conditions, see Table 1. For structures of monomers **X**, **Y**, **D** and **S**, see Figure 1.

nucleotide sequence at one position relative to the Invader probes (Figure 2b). No recognition was observed, demonstrating that Invader-mediated dsDNA-recognition proceeds with excellent binding specificity (Figure 2e).

A Change in Strategy: pcDNA with Energetic Hotspots (DSX Probes). The above results suggest that incorporation of pseudocomplementary energetic hotspots—i.e., 5′-**YD**-3′:3′-**DY**-5′ cassettes—provide less of a benefit for dsDNA-recognition than originally anticipated. At this stage, we hypothesized that the two structural elements that activate Invader and pc-DNA probes for dsDNA-recognition—i.e., the intercalator-functionalized nucleotides forming the energetic hotspots, and the pseudocomplementary base pairs between 2,6-diaminopurine and 2-thiouracil—need to be spatially separated in order to harness their full benefits. Accordingly, a series of 13-mer **DSX**-modified Invader probes were designed, i.e., double-stranded probes featuring energetic hotspots comprised of conventional Invader building block **X**, along with pseudocomplementary base pairs between regular 2,6-diaminopurine **D** and 2-thiothymine **S** monomers. The following probes were synthesized: (i) two different **DSX**-modified Invader probes, in which the energetic hotspot either is next to or one nucleotide away from two pseudocomplementary base pairs (**DSX1**:**DSX2** and **DSX3**:**DSX4**), (ii) an Invader probe comprised of regular **X** monomers (**X5**:**X6**), (iii) an Invader probe with a single pseudocomplementary energetic hotspot (**DY5**:**DY6**), and (iv) three pcDNA probes, each containing two differentially spaced, regular pseudocomplementary base pairs (**SD1**:**SD2**, **SD3**:**SD4** and **SD5**:**SD6**) (Table 3).

First, T_m's for duplexes between individual probe strands and cDNA (Table 3, first two T_m columns) or cRNA (Table S9) were determined. In line with observations from the 9-mer series, **X**-modified ONs form highly thermostable duplexes with cDNA (ΔT_m = 11−12 °C) and less thermostable duplexes with cRNA (ΔT_m = 3 °C). In comparison, ONs with **DY** motifs display slightly higher cRNA affinity (ΔT_m for **DY5**/**DY6** = 4.5−5.0 °C, Table S9) and slightly lower cDNA affinity (ΔT_m = 10 °C, Table 3), again suggesting that the normally stabilizing base-pairs between 2,6-diaminoadenosine:thymine and 2-thiouracil:adenine are weakened by proximal intercalation of the pyrene moieties. Encouragingly, **DSX**-modified ONs display significantly increased cDNA and cRNA affinity relative to **X**-modified ONs ($\Delta T_{m,DNA}$ = 14−15 °C, Table 3; $\Delta T_{m,RNA}$ = 7.0−8.5 °C, Table S9), suggesting that separation of the intercalators and the modified nucleobases is beneficial for binding affinity. In comparison, regular pcDNA strands form far less stable duplexes with cDNA ($\Delta T_{m,DNA}$ = 2.5−4.0 °C, Table 3).

Benchmark Invader probe **X5**:**X6** and **DY5**:**DY6** are both relatively thermolabile (ΔT_m = −0.5 °C and −1.5 °C, respectively, Table 3). **DSX** probes are slightly less stable (ΔT_m = −2.0 °C and −3.0 °C for **DSX1**:**DSX2** and **DSX3**:**DSX4**, respectively, Table 3). However, comparison with the corresponding pcDNA probes suggests that the full destabilizing effect of the pseudocomplementary base pairs still is not fully realized with these probe architectures (e.g., compare ΔT_m of −8.0, −0.5, and −3.0 for **SD5**:**SD6**, **X5**:**X6** and **DSX3**:**DSX4**, respectively, Table 3).

The above T_m-based conclusions are substantiated by the Gibbs free energies for formation of duplexes (Table 3). As a result of these stability trends, **DSX** probes are significantly more thermodynamically activated for dsDNA-recognition than **X5**:**X6**, **DY5**:**DY6**, or any of the regular pcDNA (trend in ΔG^{293}_{rec} values: **DSX3**:**DSX4** < **DSX1**:**DSX2** ≪ **X5**:**X6** < **DY5**:**DY6** ≪ **SD5**:**SD6** < **SD3**:**SD4** < **SD1**:**SD2**, Table 3).

Recognition of DNA Hairpins Using Energetically Activated 13-mer Probe Duplexes. On the basis of the

DOI: 10.1021/acs.joc.6b00369
J. Org. Chem. 2016, 81, 3335−3346

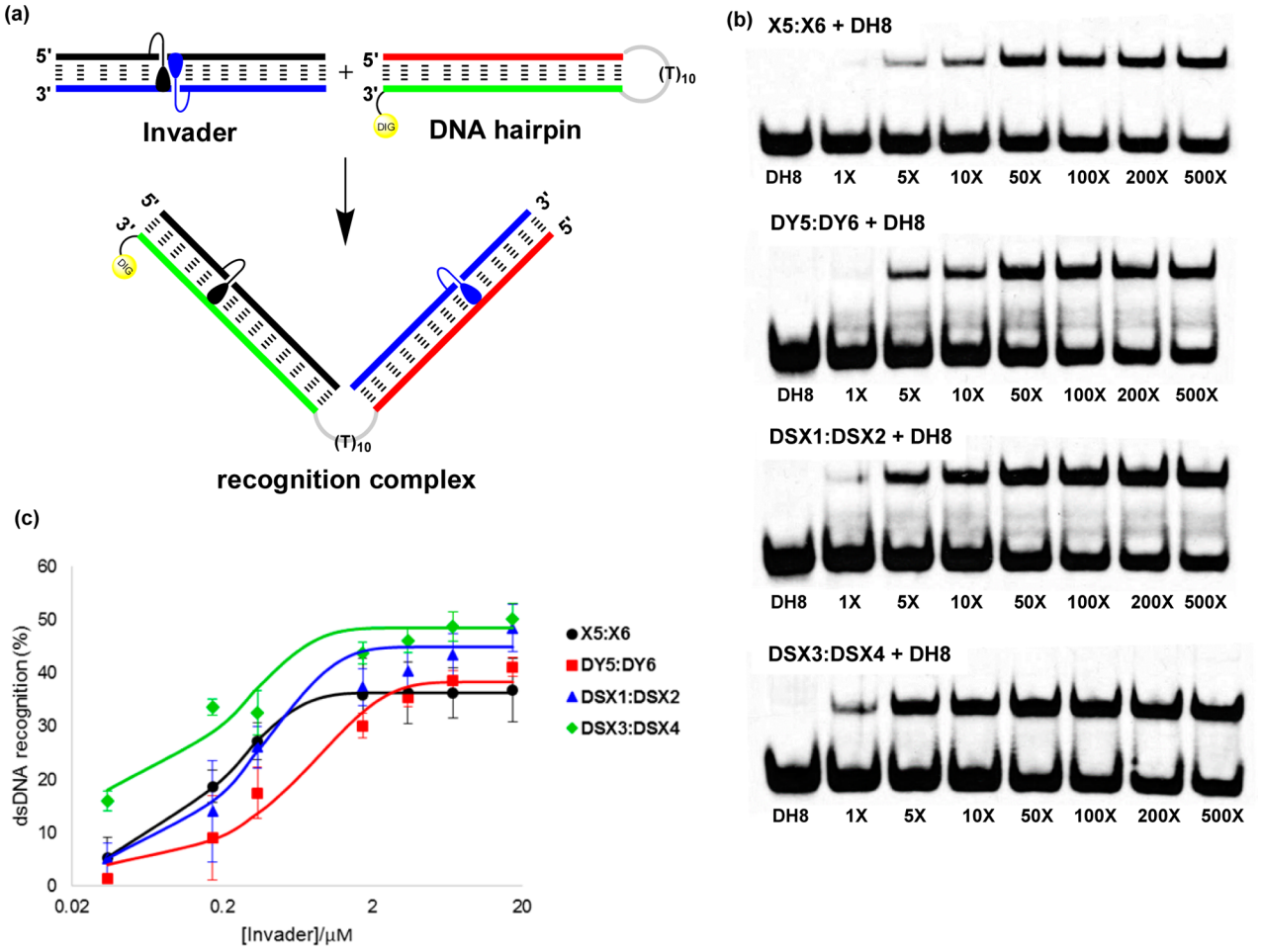

Figure 3. Recognition of dsDNA model target **DH8** using different Invader probes. (a) Illustration of recognition process; (b) representative electrophoretograms for recognition of **DH8** using 1- to 500-fold excess of **X5**:**X6**, **DY5**:**DY6** **DSX1**:**DSX2**, or **DSX3**:**DSX4**; (c) dose−response curves (average of at least three independent experiments, error bars represent standard deviation). The sequence of DNA hairpin **DH8** is shown in Figure 4. For experimental conditions, see Figure 2.

observed ΔG^{293}_{rec} values, we decided to evaluate the dsDNA-targeting efficiency of **DSX1**:**DSX2**, **DSX3**:**DSX4**, **X5**:**X6**, and **DY5**:**DY6** using a similar electrophoretic mobility shift assay as used in the 9-mer series (Figure 3a). Thus, a DIG-labeled DNA hairpin (**DH8**)—comprised of a 13-mer double-stranded mixed-sequence stem that is linked by a T_{10} loop—was used as a model dsDNA target. Incubation of **DH8** with the various 13-mer Invader probes results in dose-dependent formation of a slower moving band on nondenaturing PAGE gels (Figure 3b). As expected from the initial 9-mer studies, the parent Invader **X5**:**X6** recognizes **DH8** more effectively at low probe concentrations than **DY5**:**DY6**, which has a pseudocomplementary energetic hotspot (Figure 3c). Gratifyingly, Invader probes with separated pseudocomplementary base pairs and energetic hotspots display improved recognition efficiency (see curves for **DSX1**:**DSX2** and **DSX3**:**DSX4**, respectively, Figure 3c), which follows the observed trend in ΔG^{293}_{rec} values. It is particularly noteworthy that the use of as little as 1.0 mol equiv of **DSX3**:**DSX4** results in ∼20% recognition of **DH8**, especially when considering that optimal Invader design normally calls for incorporation of multiple energetic hotspots.[33] This suggests that spatial separation of pseudocomplementary base pairs and energetic hotspots is a promising principle for the design of efficient dsDNA-targeting Invader probes.

In the present study, we have only evaluated AT-rich DNA targets. Although there is an absence of suitable pseudocomplementary base pairs for CG-steps,[46] we have previously shown that energetic hotspots can be comprised of intercalator-functionalized monomers that are based on any of the natural nucleobases (although there is a preference for pyrimidine monomers).[30] It is, therefore, likely possible to design **DSX**-like probes against DNA targets with a higher GC-content than studied herein.

Lastly, binding specificity was studied by incubating the Invader probes with DNA hairpins **DH9**−**DH14**, which differ in the nucleotide sequence at one position in the stem region relative to the probes (Figure 4a). Excellent discrimination of the nontarget DNA hairpins is observed, even when using a 200-fold molar excess of **X5**:**X6**, **DY5**:**DY6** or **DSX1**:**DSX2** (Figure 4b). Similarly, high-affinity Invader probe **DSX3**:**DSX4** only results in trace recognition of **DH10** and **DH14**. To gain further insight into the underlying reasons for the excellent binding fidelity, we evaluated individual probe strands against singly mismatched single-stranded DNA targets (Tables S10–S12). Excellent mismatch discrimination is generally observed. In agreement with the observations from the dsDNA-recognition experiments, the discrimination is least efficient when **DSX3** or **DSX4** are hybridized with single-stranded targets that have a sequence corresponding to the target region

DOI: 10.1021/acs.joc.6b00369
J. Org. Chem. 2016, 81, 3335−3346

(a)

HP	Sequence	T_m (°C)
DH8	5' - GGTATATATAGGC 3' - CCATATATATCCG	58.0
DH9	5' - GGTATTTATAGGC 3' - CCATAAATATCCG	60.5
DH10	5' - GGTATGTATAGGC 3' - CCATACATATCCG	63.5
DH11	5' - GGTATCTATAGGC 3' - CCATAGATATCCG	63.0
DH12	5' - GGTATATAAAGGC 3' - CCATATATTTCCG	60.0
DH13	5' - GGTATATAGAGGC 3' - CCATATATCTCCG	62.5
DH14	5' - GGTATATACAGGC 3' - CCATATATGTCCG	62.5

(b)

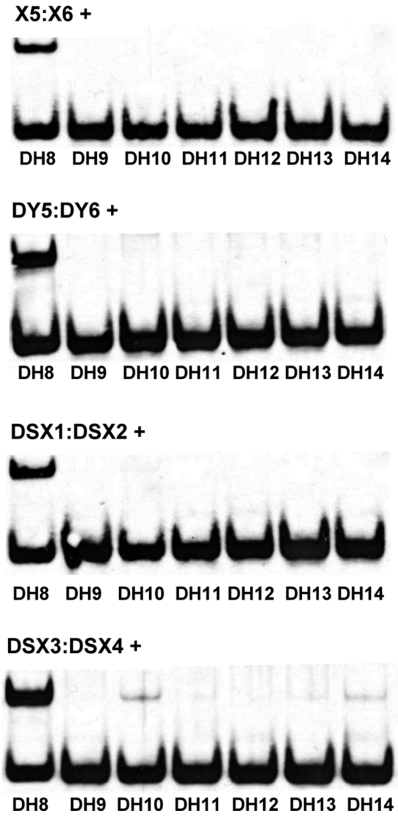

Figure 4. Recognition of mismatched DNA hairpins using various types of Invader probes. (a) Sequences and thermal denaturation temperatures of DNA hairpins with isosequential (**DH8**) or nonisosequential stems (**DH9**−**DH14**); underlined nucleotides denote sequence deviations relative to Invader probes. (b) Representative gel electrophoretograms illustrating incubation of **DH8**−**DH14** with 200-fold molar excess of **X5**:**X6**, **DY5**:**DY6**, **DSX1**:**DSX2**, or **DSX3**:**DSX4**. For experimental conditions, see Figure 2.

in **DH10** and **DH14** (T_m's only reduced by 5−7 °C, relative to matched duplexes, Table S12). The binding of Invader probes to noncomplementary dsDNA targets would accordingly entail formation of *two* mismatched and destabilized probe-target duplexes, which is energetically prohibitive in most cases. Moreover, like other structured probes, the double-stranded Invader probes are also likely to exhibit improved binding specificity due to a "stringency clamping" effect.[47,48] Thus, pseudocomplementary Invader probes allow for strong and highly specific binding to mixed-sequence dsDNA target regions at ionic conditions.

CONCLUSION

A synthetic route to 2′-*N*-(pyren-1-yl)methyl-2′-amino-2′-deoxy-2′-*N*-methyl-2-thiouridine phosphoramidite **6** has been developed (~10% overall yield over 13 steps from uridine). ONs modified with the corresponding **Y** monomer display high affinity toward cDNA (ΔT_m up to +11.5 °C). Incorporation of 2-aminoadenosine monomer **D** next to the **Y** monomer further increases cDNA affinity. Double-stranded probes with "pseudocomplementary hotspots" (i.e., 5′-**YD**-3′:3′-**DY**-5′ cassettes) are thermolabile and activated for recognition of dsDNA targets, but less so than regular Invader probes with hotspots comprised of 2′-*N*-(pyren-1-yl)methyl-2′-*N*-methyl-2′-aminouridine monomer **X**. In other words, close proximity of the two structural elements that normally activate pseudocomplementary DNA and Invader probes for dsDNA-recognition—i.e., the weak base pairs between 2,6-diaminopurine and 2-thiouracil, and the destabilizing +1 interstrand zipper arrangements of intercalating pyrene moieties—does not provide a clear design benefit. In contrast, **DSX** probes, in which the two destabilizing structural motifs are separated, are strongly activated for recognition of mixed-sequence dsDNA targets. This was confirmed in studies with model dsDNA targets as efficient recognition was demonstrated to occur with excellent specificity. Thus, the use of chimeric pseudocomplementary Invader probes presents itself as a promising strategy for mixed-sequence recognition of dsDNA for applications in molecular biology and nucleic acid diagnostics, especially since we have recently demonstrated that conventional Invader probes can recognize target regions in chromosomal DNA.[33]

EXPERIMENTAL SECTION

3′-*O*-Acetyl-2′-amino-2′-deoxy-5′-*O*-methanesulfonyl-2′-*N*-methyl-2′-*N*-(pyren-1-ylmethyl)uridine (2). Nucleoside **1**[32] (3.40 g, 4.39 mmol) was coevaporated with anhydrous 1,2-dichloroethane (2 × 30 mL), redissolved in anhydrous pyridine (55 mL) and cooled to 0 °C. To this was added 4-dimethylaminopyridine (DMAP, 55 mg, 0.44 mmol) and acetic anhydride (1.25 mL, 13.18 mmol). After stirring at ambient temperature for 12 h, the reaction mixture was diluted with EtOAc (150 mL) and washed with H_2O (80 mL) and saturated aqueous $NaHCO_3$ (80 mL). The organic layer was evaporated to near dryness and coevaporated with absolute EtOH:toluene (2:1 v/v, 3 × 30 mL). The resulting residue (~3.5 g) was suspended in AcOH:H_2O (4:1 v/v, 55 mL) and the reaction mixture was stirred overnight at room temperature. Solvents were evaporated off and the resulting residue was purified by silica gel column chromatography (0−5% MeOH/CH_2Cl_2, v/v) to afford O5′-hydroxy derivative (~1.8 g) as a white solid material. This material was coevaporated with anhydrous pyridine:CH_2Cl_2 (1:1 v/v, 2 × 30 mL), redissolved in anhydrous

DOI: 10.1021/acs.joc.6b00369
J. Org. Chem. 2016, 81, 3335−3346

pyridine:CH_2Cl_2 (1:1 v/v, 44 mL) and cooled to −20 °C (ice/salt). Methanesulfonyl chloride (0.75 mL, 9.62 mmol) was added dropwise over 30 min and the reaction mixture was stirred at −20 °C for 2 h more. The reaction mixture was diluted with CH_2Cl_2 (80 mL) and washed with saturated aqueous $NaHCO_3$ (50 mL). The aqueous layer was back-extracted with CH_2Cl_2 (3 × 15 mL) and the organic layers were combined and evaporated to dryness, followed by coevaporation with absolute EtOH:toluene (2:1 v/v, 3 × 30 mL). The resulting residue was purified by silica gel column chromatography (0−3% MeOH/CH_2Cl_2, v/v) to afford nucleoside **2** (1.43 g, 55%) as a white foam. R_f = 0.4 (5% MeOH in CH_2Cl_2, v/v); MALDI-HRMS *m/z* 614.1600 ($[M + Na]^+$, $C_{30}H_{29}N_3O_8S{\cdot}Na^+$, Calc. 614.1568); ^{1}H NMR (500 MHz, DMSO-d_6) δ 11.47 (d, 1H, ex, J = 2.2 Hz, NH), 8.33−8.36 (d, 1H, J = 9.0 Hz, Py), 8.25−8.29 (ap t, 2H, J = 7.6 Hz, Py), 8.21 (d, 1H, J = 7.5 Hz, Py), 8.15 (br s, 2H, Py), 8.10−8.12 (d, 1H, J = 9.0 Hz, Py), 8.04−8.08 (t, 1H, J = 7.6 Hz, Py), 7.92 (d, 1H, J = 7.5 Hz, Py), 7.73 (d, 1H, J = 8.2 Hz, H6), 6.40 (d, 1H, J = 7.4 Hz, H1′), 5.67 (dd, 1H, J = 8.2 Hz, 2.2 Hz, H5), 5.39 (dd, 1H, J = 6.6 Hz, 3.6 Hz, H3′), 4.44−4.48 (m, 2H, H5′), 4.34−4.43 (m, 3H, CH_2Py, H4′), 3.84 (ap t, 1H, J ∼ 7.5 Hz, H2′), 3.20 (s, 3H, CH_3SO_2), 2.34 (s, 3H, CH_3N), 2.13 (s, 3H, CH_3CO); ^{13}C NMR (125 MHz, DMSO-d_6) δ 169.7, 162.7, 150.5, 140.6 (C6), 131.9, 130.7, 130.3, 130.2, 129.1, 127.7 (Py), 127.3 (Py), 127.0 (Py), 126.8 (Py), 126.1 (Py), 125.1 (Py), 124.4 (Py), 124.2, 123.8, 123.7 (Py), 102.6 (C5), 83.7 (C1′), 80.0 (C4′), 71.7 (C3′), 69.1 (C5′), 64.9 (C2′), 57.5 (CH_2Py), 37.7 (CH_3N), 36.8 (CH_3SO_2), 20.9 (CH_3CO).

2′-Amino-2′-deoxy-2-*O*-ethyl-2′-*N*-methyl-2′-*N*-(pyren-1-ylmethyl)uridine (3). Nucleoside **2** (0.77 g, 1.30 mmol) was dried through coevaporation with anhydrous 1,2-dichloroethane (3 × 6 mL) and suspended in anhydrous EtOH (25 mL). To this was added $NaHCO_3$ (275 mg, 3.25 mmol) and the reaction mixture was refluxed for 4 days. CH_2Cl_2 (100 mL) was added and the precipitate was filtered off and washed with CH_2Cl_2. The combined organic layers were evaporated to dryness and the resulting residue was purified via silica gel column chromatography (0−7% MeOH in CH_2Cl_2, v/v) to afford nucleoside **3** (0.34 g, 52%) as a white foam. R_f = 0.3 (10% MeOH in CH_2Cl_2, v/v); MALDI-HRMS *m/z* 522.1985 ($[M + Na]^+$, $C_{29}H_{29}N_3O_5{\cdot}Na^+$, Calc. 522.1999); ^{1}H NMR (500 MHz, DMSO-d_6) δ 8.39−8.42 (d, 1H, J = 9.3 Hz, Py), 8.24−8.28 (m, 2H, Py), 8.19−8.22 (d, 1H, J = 8.0 Hz, Py), 8.14 (br s, 2H, Py), 8.03−8.10 (d+t, 2H, Py), 7.96−7.99 (d, 1H, J = 8.0 Hz, Py), 7.93 (d, 1H, J = 7.7 Hz, H6), 6.35 (d, 1H, J = 8.5 Hz, H1′), 5.83 (d, 1H, J = 7.7 Hz, H5), 5.53 (d, 1H, ex, J = 4.9 Hz, 3′−OH), 5.12 (t, 1H, ex, J = 5.2 Hz, 5′−OH), 4.43−4.51 (m, 3H, CH_2Py, H3′), 4.12−4.27 (m, 2H, O$\underline{CH_2}CH_3$), 3.99−4.01 (m, 1H, H4′), 3.58−3.62 (m, 2H, H5′), 3.47 (dd, 1H, J = 8.5 Hz, 5.2 Hz, H2′), 2.36 (s, 3H, CH_3N), 1.06 (t, 3H, J = 7.1 Hz, $\underline{CH_3}CH_2O$); ^{13}C NMR (125 MHz, DMSO-d_6) δ 169.3, 155.0, 138.1 (C6), 132.7, 130.7, 130.3, 130.1, 129.0, 127.5 (Py), 127.3 (Py), 126.9 (Py), 126.8 (Py), 126.1 (Py), 125.02 (Py), 124.99 (Py), 124.4 (Py), 124.1, 123.8, 123.6 (Py), 108.4 (C5), 87.6 (C4′), 85.0 (C1′), 71.2 (C3′), 68.8 (C2′), 64.2 (O$\underline{CH_2}CH_3$), 61.7 (C5′), 57.1 (CH_2Py), 39.0 (CH_3N − overlap with DMSO-d_6 signal), 13.6 ($\underline{CH_3}CH_2O$).

2′-Amino-2′-deoxy-5′-*O*-(4,4′-dimethoxytrityl)-2-*O*-ethyl-2′-*N*-methyl-2′-*N*-(pyren-1-ylmethyl)uridine (4). Nucleoside **3** (0.32 g, 0.63 mmol) was coevaporated with anhydrous 1,2-dichloroethane (2 × 5 mL) and redissolved in anhydrous pyridine (6 mL). To this was added DMTrCl (0.26 g, 0.76 mmol) and 4-dimethylaminopyridine (DMAP, 8 mg, 0.06 mmol) and the reaction mixture was stirred at ambient temperature for 14 h at which point it was diluted with $CHCl_3$ (80 mL) and washed with saturated aqueous $NaHCO_3$ (30 mL) and H_2O (30 mL). The aqueous layer was back-extracted with $CHCl_3$ (3 × 15 mL) and the combined organic layers were dried (Na_2SO_4) and evaporated to dryness. The resulting residue was purified by silica gel column chromatography (0−2.5% MeOH in $CHCl_3$, v/v) to afford nucleoside **4** (0.45 g, 88%) as a pale orange foam. R_f = 0.7 (10% MeOH in CH_2Cl_2, v/v); MALDI-HRMS *m/z* 824.3319 ($[M + Na]^+$, $C_{50}H_{47}N_3O_7{\cdot}Na^+$, Calc. 824.3306); ^{1}H NMR (500 MHz, DMSO-d_6) δ 8.38−8.41 (d, 1H, J = 9.3 Hz, Py), 8.25−8.29 (m, 2H, Py), 8.17−8.19 (d, 1H, J = 7.8 Hz, Py), 8.11−8.15 (2d, 2H, J = 9.1 Hz, 9.1 Hz, Py), 8.04−8.09 (m, 2H, Py), 7.98−8.00 (d, J = 7.8 Hz, Py), 7.69 (d, 1H, J = 7.8 Hz, H6), 7.19−7.38 (m, 9H, DMTr), 6.83−6.88 (m, 4H, DMTr), 6.32 (d, 1H, J = 7.9 Hz, H1′), 5.60−5.64 (m, 2d, 1 ex, J = 7.8 Hz, 5.0 Hz, H5, 3′−OH), 4.48−4.54 (m, 2H, CH_2Py), 4.44−4.48 (m, 1H, H3′), 4.10−4.24 (m, 3H, H4′, O$\underline{CH_2}CH_3$), 3.71 (s, 3H, CH_3O), 3.70 (s, 3H, CH_3O), 3.52−3.58 (dd, 1H, J = 7.9 Hz, 5.8 Hz, H2′), 3.31−3.35 (dd, 1H, J = 10.5 Hz, 5.0 Hz, H5′ - partial overlap with H_2O), 3.15−3.20 (dd, 1H, J = 10.5 Hz, 3.5 Hz, H5′), 2.43 (s, 3H, CH_3N), 1.05 (t, 3H, J = 7.0 Hz, $\underline{CH_3}CH_2O$); ^{13}C NMR (125 MHz, DMSO-d_6) δ 169.2, 158.09, 158.08, 154.9, 144.5, 138.1 (C6), 135.3, 135.0, 132.6, 130.7, 130.2, 130.1, 129.7 (DMTr), 129.6 (DMTr), 129.0, 127.8 (DMTr), 127.6 (DMTr), 127.5 (Py), 127.3 (Py), 126.91 (Py), 126.86 (Py), 126.7 (DMTr), 126.1 (Py), 125.0 (Py), 124.4 (Py), 124.1, 123.9, 123.6 (Py), 113.20 (DMTr), 113.17 (DMTr), 108.1 (C5), 85.9, 85.7 (C4′), 85.3 (C1′), 71.0 (C3′), 68.1 (C2′), 64.2 (O$\underline{CH_2}CH_3$), 64.0 (C5′), 57.1 (CH_2Py), 55.0 (CH_3O), 38.8 (CH_3N), 13.6 ($\underline{CH_3}CH_2O$). A trace impurity of $CHCl_3$ was identified in the ^{13}C NMR at 79.1 ppm.[49]

2′-Amino-2′-deoxy-5′-*O*-(4,4′-dimethoxytrityl)-2′-*N*-methyl-2′-*N*-(pyren-1-ylmethyl)-2-thiouridine (5). An ice-cold solution of anhydrous 1,1,3,3-tetramethylguanidine (TMG, 0.68 mL, 5.42 mmol) in anhydrous pyridine (10 mL) was saturated with hydrogen sulfide gas for 1 h while maintaining the temperature at 0 °C. The solution was transferred, using an argon-flushed syringe, to a precooled flask containing nucleoside **4** (0.44 g, 0.54 mmol) and the reaction mixture was allowed to reach room temperature. After stirring under an argon atmosphere for 72 h, EtOAc (100 mL) was added and the organic layer was washed with saturated aqueous $NaHCO_3$ (50 mL) and H_2O (50 mL). The aqueous layer was back-extracted with CH_2Cl_2 (3 × 20 mL) and the combined organic layers were evaporated to dryness and coevaporated with absolute EtOH:toluene (2:1 v/v, 3 × 15 mL). The resulting residue was purified by silica gel column chromatography (0−70% EtOAc in petroleum ether, v/v) to afford nucleoside **5** (0.35 g, 82%) as a white foam. R_f = 0.8 (80% EtOAc in petroleum ether, v/v); MALDI-HRMS *m/z* 812.2765 ($[M + Na]^+$, $C_{48}H_{43}N_3O_6S{\cdot}Na^+$, Calc. 812.2797); ^{1}H NMR (500 MHz, DMSO-d_6) δ 12.77 (br s, 1H, ex, NH), 8.49−8.52 (d, 1H, J = 9.3 Hz, Py), 8.24−8.29 (m, 2H, Py), 8.17−8.20 (d, 1H, J = 8.0 Hz, Py), 8.12−8.16 (2d, 2H, J = 9.1 Hz, 9.1 Hz, Py), 8.02−8.11 (m, 3H, Py), 7.75 (d, 1H, J = 8.2 Hz, H6), 7.20−7.39 (m, 10H, DMTr, H1′), 6.84−6.89 (m, 4H, DMTr), 5.62 (dd, 1H, J = 8.2 Hz, 1.7 Hz, H5), 5.55 (d, 1H, ex, J = 4.9 Hz, 3′−OH), 4.53−4.57 (d, 1H, J = 13.0 Hz, CH_2Py), 4.43−4.51 (m, 2H, CH_2Py, H3′), 4.08−4.12 (m, 1H, H4′), 3.71 (s, 3H, CH_3O), 3.70 (s, 3H, CH_3O), 3.48−3.52 (m, 1H, H2′), 3.33−3.37 (dd, 1H, J = 10.5 Hz, 5.0 Hz, H5′), 3.18−3.22 (dd, 1H, J = 10.5 Hz, 3.0 Hz, H5′), 2.44 (s, 3H, CH_3N); ^{13}C NMR (125 MHz, DMSO-d_6) δ 176.6, 159.0, 158.11, 158.10, 144.5, 140.8 (C6), 135.3, 135.0, 132.6, 130.7, 130.3, 130.2, 129.73 (DMTr), 129.68 (DMTr), 129.2, 128.0 (Py), 127.9 (DMTr), 127.6 (DMTr), 127.3 (Py), 127.0 (Py), 126.8 (Py), 126.7 (DMTr), 126.1 (Py), 125.02 (Py), 125.00 (Py), 124.4 (Py), 124.1, 124.0 (Py), 123.9, 113.3 (DMTr), 113.2 (DMTr), 106.9 (C5), 88.0 (C1′), 86.0, 85.4 (C4′), 71.0 (C3′), 68.6 (C2′), 63.9 (C5′), 57.6 (CH_2Py), 55.0 (CH_3O), 39.2 (CH_3N; overlap with DMSO-d_6).

2′-Amino-2′-deoxy-3′-*O*-(*N*,*N*-diisopropylamino-2-cyanoethoxyphosphinyl)-5′-*O*-(4,4′-dimethoxytrityl)-2′-*N*-methyl-2′-*N*-(pyren-1-ylmethyl)-2-thiouridine (6). To a flame-dried round-bottomed flask containing nucleoside **5** (150 mg, 0.19 mmol) was added anhydrous CH_2Cl_2 (2 mL), anhydrous *N*,*N*-diisopropylethylamine (DIPEA, 165 μL, 0.95 mmol) and 2-cyanoethyl-*N*,*N*-diisopropylchlorophosphoramidite (PCl reagent, 85 μL, 0.38 mmol). The reaction mixture was stirred at room temperature for 3.5 h at which point ice-cold EtOH (1.0 mL) was added. The reaction mixture was evaporated to dryness and the resulting residue was purified by silica gel column chromatography (0−55% EtOAc in petroleum ether, v/v) followed by precipitation from cold petroleum ether to afford nucleoside **6** (153 mg, 81%) as a white foam. R_f = 0.6 (50% EtOAc in petroleum ether, v/v); MALDI-HRMS *m/z* 1012.3843 ($[M + Na]^+$, $C_{57}H_{60}N_5O_7PS{\cdot}Na^+$, Calc. 1012.3887); ^{31}P NMR (121 MHz, $CDCl_3$) δ 150.9, 149.6.

Protocol: Synthesis and Purification of ONs. Modified ONs were synthesized on a 0.2 μmol scale using a DNA synthesizer,

DOI: 10.1021/acs.joc.6b00369
J. Org. Chem. 2016, 81, 3335−3346

succinyl-linked LCAA-CPG (long chain alkyl amine controlled pore glass) columns with a pore size of 500 Å, and standard protocols for incorporation of A^{Bz}, C^{Bz}, G^{iBu} and T DNA phosphoramidites. The following hand-coupling conditions were used for incorporation of the corresponding phosphoramidites of monomers **X**, **Y**, **S** (N3/O4-toluoyl protected) and **D** (bis(diisobutylaminomethylidene)-protected) (coupling time; activator; coupling yield): **X** (15 min; 5-[3,5-bis(trifluoromethyl)phenyl]-1*H*-tetrazole; ~99%), **Y** (15 min; 4,5-dicyanoimidazole; ~95%) and **S**/**D** (15 min; 4,5-dicyanoimidazole; ~99%). Modified phosphoramidites were used at 50-fold molar excess and 0.05 M concentration in CH_3CN. Extended oxidation (45 s) with standard 0.05 M aqueous iodine was used for **D1**−**D4** and **X1**−**X6**. Extended oxidation (2 × 5 min oxidation with an acetonitrile wash between oxidations) using a *tert*-butylhydroperoxide/CH_3CN/H_2O solution (10/87/3, v/v/v) was used for all ONs containing **S** and **Y** modifications to prevent desulfurization.[40] Cleavage from solid support and removal of protecting groups was accomplished by treatment with 32% aq. ammonia (55 °C, 16−24 h). ONs were purified in the DMT-on mode via ion-pair reverse phase HPLC (C_{18} column) using a 0.05 M triethylammonium acetate−water/acetonitrile gradient. This was followed by detritylation (80% aq. AcOH) and precipitation (NaOAc/$NaClO_4$/acetone, −18 °C for 12−16 h). The identity of synthesized ONs was established through MALDI-MS analysis (Table S1) recorded in positive ions mode on a quadrupole time-of-flight tandem mass spectrometer equipped with a MALDI source using anthranilic acid, 3-hydroxypicolinic acid (3-HPA) or 2,4,6-trihydroxyacetophenone (THAP) as matrices. Purity was verified by ion-pair reverse phase HPLC running in analytical mode (>90% unless otherwise mentioned).

Protocol: Thermal Denaturation Studies. ON concentrations were estimated using the following extinction coefficients for DNA (OD/μmol): G (12.01), A (15.20), T (8.40), C (7.05); RNA (OD/μmol): G (13.70), A (15.40), U (10.00), C (9.00); pyrene (22.4),[50] **D** (8.5), **S** (10.0) and **Y** (32.4).[51] Strands were thoroughly mixed and denatured by heating to 70−85 °C, followed by cooling to the starting temperature of the experiment. Quartz optical cells with a path length of 1.0 cm were used. Thermal denaturation temperatures (T_m's) of duplexes (1.0 μM final concentration of each strand) were measured using a UV/vis spectrophotometer equipped with a 12-cell Peltier temperature controller and determined as the maximum of the first derivative of thermal denaturation curves (A_{260} vs T) recorded in medium salt phosphate buffer (T_m buffer: 100 mM NaCl, 0.1 mM EDTA and pH 7.0 adjusted with 10 mM Na_2HPO_4 and 5 mM Na_2HPO_4). The temperature of the denaturation experiments ranged from at least 15 °C below T_m to 20 °C above T_m (although not below 3 °C). A temperature ramp of 0.5 °C/min was used in all experiments. Reported T_m's are averages of two experiments within ±1.0 °C.

Protocol: Determination of Thermodynamic Parameters. Thermodynamic parameters for duplex formation were determined through fitting of baselines of denaturation curves (van't Hoff analysis) using software provided with the UV/vis spectrometer. Bimolecular reactions, two-state melting behavior, and a heat capacity change of $\Delta C_p = 0$ upon hybridization were assumed.[44] A minimum of two experimental denaturation curves were each analyzed at least three times to minimize errors arising from baseline choice. Averages and standard deviations are listed.

Protocol: Absorption Spectra. UV−vis absorption spectra (range 200−600 nm) were recorded at 10 °C using the same samples and instrumentation as in the thermal denaturation experiments.

Protocol: Steady-State Fluorescence Emission Spectra. Steady-state fluorescence emission spectra of **Y**- or **DY**-modified ONs and the corresponding duplexes with complementary DNA/RNA targets, were recorded in nondeoxygenated thermal denaturation buffer (each strand at 1.0 μM concentration) and obtained as an average of five scans using an excitation wavelength of λ_{ex} = 350 nm. Excitation and emission slits of 5.0 and 2.5 nm, respectively, were used along with a scan speed of 600 nm/min. Experiments were determined at 5 °C (to ascertain maximal hybridization of probes to DNA/RNA targets) under N_2 flow (to prevent condensation).

Protocol: Electrophoretic Mobility Shift Assay. This assay was performed essentially as previously described.[29] Unmodified DNA hairpins **DH1**−**DH14** were obtained from commercial sources and used without further purification. The DNA hairpins were 3′-DIG-labeled using the second generation DIG Gel Shift Kit (Roche Applied Bioscience) following the manufacturer's recommendation. DIG-labeled ONs obtained in this manner were diluted and used without further purification in the recognition experiments. Preannealed probes (85 °C for 10 min, cooled to room temperature over 15 min) and DIG-labeled DNA hairpins (34.4 nM) were mixed and incubated in HEPES buffer (50 mM HEPES, 100 mM NaCl, 5 mM $MgCl_2$, 10% sucrose, 1.44 mM spermine tetrahydrochloride, pH 7.2) for the specified time at ambient temperature (~21 ± 3 °C). The reaction mixtures were then diluted with 6x DNA loading dye (Fermentas) and loaded onto a 16% nondenaturing polyacrylamide gel. Electrophoresis was performed using a constant voltage of 70 V for 2.5 h at ~4 °C using 0.5× TBE as a running buffer (45 mM Tris, 45 mM boric acid, 1 mM EDTA). Gels were blotted onto positively charged nylon membranes (Roche Applied Bioscience) using constant voltage with external cooling (100 V, ~4 °C). The membranes were exposed to antidigoxigenin-AP F_{ab} fragments as recommended by the manufacturer of the DIG Gel Shift Kit, transferred to a hybridization jacket, and incubated with the substrate (CSPD) in detection buffer for 10 min at 37 °C. The chemiluminescence of the formed product was captured on X-ray film, which was developed using an X-Omatic 1000A X-ray film developer (Kodak). The resulting bands were quantified using ImageJ software. The efficiency of DNA recognition was determined as the intensity ratio between the recognition complex band and the total lane. An average of three independent measurements is reported along with standard deviations. Nonlinear regression was used to fit data points from dose−response experiments, using a script written for the "Solver" module in Microsoft Office Excel.[52]

Definition of Zipper Nomenclature. The following nomenclature describes the relative arrangement between two pyrene-functionalized monomers positioned on opposing strands in a duplex: The number n describes the distance measured in number of base pairs and has a positive value if a monomer is shifted toward the 5′-side of its own strand relative to a second reference monomer on the other strand. Conversely, n has a negative value if a monomer is shifted toward the 3′-side of its own strand relative to a second reference monomer on the other strand.

■ ASSOCIATED CONTENT

Supporting Information

The Supporting Information is available free of charge on the ACS Publications website at DOI: 10.1021/acs.joc.6b00369.

General experimental section; NMR spectra for new compounds; MS data for new modified ONs; representative T_m curves; additional thermal denaturation, UV−vis absorption, steady-state fluorescence emission, thermodynamic parameter and dsDNA recognition data. (PDF)

■ AUTHOR INFORMATION

Corresponding Author

*E-mail: hrdlicka@uidaho.edu.

Notes

The authors declare no competing financial interest.

■ ACKNOWLEDGMENTS

This study was supported by Award Number GM088697 from the National Institute of General Medical Sciences, National Institutes of Health and by Grant No. 12658-I from the University of Idaho Student Grant Program. We thank Dr. Alex Blumenfeld (Dept. Chemistry, Univ. Idaho) and Dr. Lee

DOI: 10.1021/acs.joc.6b00369
J. Org. Chem. 2016, 81, 3335−3346

Deobald (EBI Murdock Mass Spectrometry Center, Univ. Idaho) for assistance with NMR and mass spectrometric analysis, and Prof. Carolyn Hovde (Food Science, Univ. Idaho) for access to gel documentation stations. Dr. Dale C. Guenther and Ms. Grace H. Anderson (Dept. Chemistry, Univ. Idaho) are thanked for making **X**-modified ONs available for this study.

■ DEDICATION

This article is dedicated to the memory of Prof. Leszek Czuchajowski (Univ. Idaho): Pole, poet, and professor.

■ REFERENCES

(1) Duca, M.; Vekhoff, P.; Oussedik, K.; Halby, L.; Arimondo, P. B. *Nucleic Acids Res.* **2008**, *36*, 5123−5138.
(2) Kaihatsu, K.; Janowski, B. A.; Corey, D. R. *Chem. Biol.* **2004**, *11*, 749−758.
(3) Nielsen, P. E. *Chem. Biodiversity* **2010**, *7*, 786−804.
(4) Dervan, P. B.; Edelson, B. S. *Curr. Opin. Struct. Biol.* **2003**, *13*, 284−299.
(5) Blackledge, M. S.; Melander, C. *Bioorg. Med. Chem.* **2013**, *21*, 6101−6114.
(6) Hari, Y.; Obika, S.; Imanishi, T. *Eur. J. Org. Chem.* **2012**, *2012*, 2875−2887 and references cited herein.
(7) Horne, D. A.; Dervan, P. B. *J. Am. Chem. Soc.* **1990**, *112*, 2435−2437.
(8) Filichev, V. V.; Nielsen, C.; Bomholt, C. H.; Pedersen, E. B. *Angew. Chem., Int. Ed.* **2006**, *45*, 5311−5315.
(9) Kaihatsu, K.; Shah, R. H.; Zhao, X.; Corey, D. R. *Biochemistry* **2003**, *42*, 13996−14003 and reference 39 cited herein.
(10) Bahal, R.; Sahu, B.; Rapireddy, S.; Lee, C.-M.; Ly, D. H. *ChemBioChem* **2012**, *13*, 56−60.
(11) Bohländer, P. R.; Vilaivan, T.; Wagenknecht, H.-A. *Org. Biomol. Chem.* **2015**, *13*, 9223−9230.
(12) Gaj, T.; Gersbach, C. A.; Barbas, C. F., III *Trends Biotechnol.* **2013**, *31*, 397−405.
(13) Cox, D. B. T.; Platt, R. J.; Zhang, F. *Nat. Med.* **2015**, *21*, 121−131.
(14) Sander, J. D.; Joung, J. K. *Nat. Biotechnol.* **2014**, *32*, 347−355.
(15) Fu, Y.; Sander, J. D.; Reyon, D.; Cascio, V. M.; Joung, J. K. *Nat. Biotechnol.* **2014**, *32*, 279−284.
(16) Kutyavin, I. V.; Rhinehart, R. L.; Lukhtanov, E. A.; Gorn, V. V.; Meyer, R. B., Jr.; Gamper, H. B. *Biochemistry* **1996**, *35*, 11170−11176.
(17) Lohse, J.; Dahl, O.; Nielsen, P. E. *Proc. Natl. Acad. Sci. U. S. A.* **1999**, *96*, 11804−11808.
(18) Ishizuka, T.; Yoshida, J.; Yamamoto, Y.; Sumaoka, J.; Tedeschi, T.; Corradini, R.; Sforza, S.; Komiyama, M. *Nucleic Acids Res.* **2008**, *36*, 1464−1471.
(19) Sumaoka, J.; Komiyama, M. *Chem. Lett.* **2014**, *43*, 1581−1583.
(20) Hrdlicka, P. J.; Kumar, T. S.; Wengel, J. *Chem. Commun.* **2005**, 4279−4281.
(21) Filichev, V. V.; Vester, B.; Hansen, L. H.; Pedersen, E. B. *Nucleic Acids Res.* **2005**, *33*, 7129−7137.
(22) Sau, S. P.; Madsen, A. S.; Podbevsek, P.; Andersen, N. K.; Kumar, T. S.; Andersen, S.; Rathje, R. L.; Anderson, B. A.; Guenther, D. C.; Karmakar, S.; Kumar, P.; Plavec, J.; Wengel, J.; Hrdlicka, P. J. *J. Org. Chem.* **2013**, *78*, 9560−9570.
(23) NMR structures of DNA duplexes with adjacent incorporations of intercalator-modified non-nucleotide monomers also exhibit signs of duplex unwinding and destabilization, see: Nielsen, C. B.; Petersen, M.; Pedersen, E. B.; Hansen, P. E.; Christensen, U. B. *Bioconjugate Chem.* **2004**, *15*, 260−269.
(24) Crothers, D. M. *Biopolymers* **1968**, *6*, 575−584.
(25) Tsai, C.; Jain, S. C.; Sobell, H. M. *J. Mol. Biol.* **1977**, *114*, 301−315.
(26) Williams, L. D.; Egli, M.; Gao, Q.; Rich, A. In *Structure and Function: Nucleic Acids*; Sarma, R. H., Sarma, M. H., Eds.; Adenine Press, 1992; Vol. *1*, pp 107−125.
(27) Sau, S. P.; Kumar, T. S.; Hrdlicka, P. J. *Org. Biomol. Chem.* **2010**, *8*, 2028−2036.
(28) Denn, B.; Karmakar, S.; Guenther, D. C.; Hrdlicka, P. J. *Chem. Commun.* **2013**, *49*, 9851−9853.
(29) Didion, B. A.; Karmakar, S.; Guenther, D. C.; Sau, S. P.; Verstegen, J. P.; Hrdlicka, P. J. *ChemBioChem* **2013**, *14*, 1534−1538.
(30) Karmakar, S.; Guenther, D. C.; Hrdlicka, P. J. *J. Org. Chem.* **2013**, *78*, 12040−12048.
(31) Karmakar, S.; Madsen, A. S.; Guenther, D. C.; Gibbons, B. C.; Hrdlicka, P. J. *Org. Biomol. Chem.* **2014**, *12*, 7758−7773.
(32) Anderson, B. A.; Onley, J. J.; Hrdlicka, P. J. *J. Org. Chem.* **2015**, *80*, 5395−5406.
(33) Guenther, D. C.; Anderson, G. H.; Anderson, B. A.; Karmakar, S.; Hrdlicka, P. J. *Chem. Sci.* **2015**, *6*, 5006−5015.
(34) Anderson, B. A.; Hrdlicka, P. J. *Bioorg. Med. Chem. Lett.* **2015**, *25*, 3999−4004.
(35) Anderson, B. A.; Karmakar, S.; Hrdlicka, P. J. *Molecules* **2015**, *20*, 13780−13793.
(36) Guenther, D. C.; Karmakar, S.; Hrdlicka, P. J. *Chem. Commun.* **2015**, *51*, 15051−15054.
(37) Rajeev, K. G.; Prakash, T. P.; Manoharan, M. *Org. Lett.* **2003**, *5*, 3005−3008.
(38) Reese, C. B.; Varaprasad, C. V. N. S. *J. Chem. Soc., Perkin Trans. 1* **1994**, 189−195.
(39) Karmakar, S.; Anderson, B. A.; Rathje, R. L.; Andersen, S.; Jensen, T.; Nielsen, P.; Hrdlicka, P. J. *J. Org. Chem.* **2011**, *76*, 7119−7131.
(40) Kumar, R. K.; Davis, D. R. *J. Org. Chem.* **1995**, *60*, 7726−7727.
(41) Nakamura, M.; Fukunaga, Y.; Sasa, K.; Ohtoshi, Y.; Kanaori, K.; Hayashi, H.; Nakano, H.; Yamana, K. *Nucleic Acids Res.* **2005**, *33*, 5887−5895.
(42) Azhikina, T.; Veselovskaya, S.; Myasnikov, V.; Potapov, V.; Ermolayeva, O.; Sverdlov, E. *Proc. Natl. Acad. Sci. U. S. A.* **1993**, *90*, 11460−11462.
(43) Sproat, B. S.; Lamond, A. I. *Antisense Research and Applications*; CRC Press: Boca Raton, FL, 1993.
(44) Mergny, J. L.; Lacroix, L. *Oligonucleotides* **2003**, *13*, 515−537.
(45) Asanuma, H.; Fujii, T.; Kato, T.; Kashida, H. *J. Photochem. Photobiol., C* **2012**, *13*, 124−135.
(46) Woo, J.; Meyer, R. B., Jr; Gamper, H. B. *Nucleic Acids Res.* **1996**, *24*, 2470−2475.
(47) Demidov, V. V.; Frank-Kamenetskii, M. *Trends Biochem. Sci.* **2004**, *29*, 62−71.
(48) Chen, S. X.; Zhang, D. Y.; Seelig, G. *Nat. Chem.* **2013**, *5*, 782−789.
(49) Gottlieb, H. E.; Kotlyar, V.; Nudelman, H. *J. Org. Chem.* **1997**, *62*, 7512−7515.
(50) Dioubankova, N. N.; Malakhov, A. D.; Stetsenko, D. A.; Gait, M. J.; Volynsky, P. E.; Efremov, R. G.; Korshun, V. A. *ChemBioChem* **2003**, *4*, 841−847.
(51) The A_{260} extinction coefficients for the **D** and **S** monomers were obtained from commercial vendor, whereas the A_{260} extinction coefficient for monomer **Y** was estimated to be the sum of A_{260} extinction coefficients for the pyrene moiety[50] and monomer **S**.
(52) Brown, A. M. *Comput. Methods Prog. Biol.* **2001**, *65*, 181−200.

DOI: 10.1021/acs.joc.6b00369
J. Org. Chem. 2016, 81, 3335−3346